Appl. Chem. Eng., Vol. 33, No. 3, June 2022, 315-321
https://doi.org/10.14478/ace.2022.1020

Article

Atomic Layer Deposition of Vanadium Pentoxide on Carbon Electrode for Enhanced Capacitance Performance in Capacitive Deionization

Sangho Chung[*,1], **Sungyool Bong**[*,**,***,1] **and Jaeyoung Lee**[*,**,***,†]

[*]*School of Earth Sciences and Environmental Engineering, Gwangju Institute of Science and Technology, Gwangju 61005, Korea*
[**]*International Future Research Center of Chemical Energy Storage and Conversion Processes, Gwangju Institute of Science and Technology, Gwangju 61005, Korea*
[***]*Ertl Center for Electrochemistry and Catalysis, Gwangju Institute of Science and Technology, Gwangju 61005, Korea*
(Received April 13, 2022; Revised May 13, 2022; Accepted May 16, 2022)

Abstract

We firstly observed that activated carbon (AC) deposited by atomic-layer vanadium pentoxide (V_2O_5) was used as CDI electrodes to utilize the high dielectric constant for enhancing the capacitance equipped with atomic layer deposition (ALD). It was demonstrated that the vanadium pentoxide (V_2O_5) with sub-nanometer layer was effectively deposited onto activated carbon, and the electric double-layer capacitance of the AC was improved due to an increase in the surface charge density originated from polarization, leading to high ion removal in CDI operation. It was confirmed that the performance of modified-AC increases more than 200%, comparable to that of pristine-AC under 1.5 V at 20 mL min^{-1} in CDI measurements.

Keywords: *Vanadium pentoxide, Carbon electrode, Atomic layer deposition, Capacitance deionization, Activated carbon*

1. Introduction

The water demand is continuously increasing, and desalination is one of the keys to solve this problem. Moreover, capacitive deionization (CDI) is currently studied since it has many benefits like low energy consumption, easy operation, and environment-friendly process as one of the applicable desalination technologies[1-4]. CDI cell consists of a pair of porous electrodes with a separator. The carbon electrodes are widely employed, and the blackish water flows between the charging electrodes. CDI relies on the electrochemical process which involves the adsorption of ions towards an electrode, and this separation mechanism is described by the electric double layer models proposed independently by H. Helmholtz in 1883[5]. When each electrode is charged, a negatively/positively charged layer in the electrode and a positively/negatively charged layer of ions in the solution makes the "double layer." The ion storage of the interface between the electrode and electrolyte can be possible due to the electrostatic force with the applied electric field. Consequently, ions are physically adsorbed on the porous electrode, thereby removing the ions from the blackish water[6,7].

On the contrary, adsorbed ions can be eliminated by the applied electric field or reversed by the polarity of the electrodes from the saturated electrodes. Therefore, CDI performance is strongly related to the surface properties of the electrode. CDI systems have suggested the following electrode material characteristics for more efficient ion removal.

For these reasons, the morphology and structure of electrode material are crucial factors in CDI performance[1]. Carbonaceous materials have been highly suitable for one of the candidates as the CDI electrode. Many carbons and their modification methods - activated carbon (AC) made from wood, coconut shell, oil palm wood, and coal pyrolyzed inert atmoshphere[8-11], carbon aerogels[12,13], graphene[14-16], carbon nanotube (CNT)[17,18] and carbon-polymer composite[19,20] - have been introduced for CDI electrode in the water management system. In addition, they have recently been suggested through several strategies to enhance the desalination efficiency of activated carbon electrodes. In the various carbons, it was reported that surface modification treatment of activated carbons with nitric acid[21], sulfuric acid[22], and sodium hydrochlorite[23] was introduced to increase reactive surface area, respectively. Surface modification not only made oxygen on the surface of carbon materials with functional groups increase which diminished charge resistance and enhanced capacitance, but also capacitance of electrode increase corresponding to micro-pore and surface area increase. However, the extremely high specific surface area does not increase the capacitance anymore[6] since micropores (< 2 nm) are not optimal in their adsorption/desorption performance, caused by slow mass transfer rate even if they have a large surface area[7]. The total specific capacitance can be represented in the following equation:

1 These authors contributed equally to this work.

† Corresponding Author: Gwangju Institute of Science and Technology (GIST) School of Earth Sciences and Environmental Engineering, Gwangju 61005, South Korea
Tel: +82-62-715-2440 e-mail: jaeyoung@gist.ac.kr

pISSN: 1225-0112 eISSN: 2288-4505

$$C = \varepsilon_r \varepsilon_0 \frac{A}{D} \quad (1)$$

Where C is the capacitance, ε_r is the relative static permittivity, ε_0 is the permittivity of free space, A is the electrode specific surface area, D is the separation between the plates. Therefore, it can be accessed by the following two methods to increase the capacitance.

1. Geometric method which can enlarge the specific surface area
2. Dielectric constant method by changing the properties of the material

So far, the main study was carried out to enlarge the specific surface area to increase the effective surface area. It can be formed in electric double layer capacitance (EDLC). However, this way is no longer a limitation in increasing the capacitance, and it may have trouble applying to the actual system due to very slow adsorption/desorption. To overcome this limitation, we tried to approach the electrode to increase the dielectric constant instead of the specific surface area. Generally, the dielectric constant materials are non-conductive materials, which means they are not appropriate as CDI electrodes. Vanadium pentoxide (V_2O_5) was considered as a talented material that was widely used for oxidation and dehydrogenation of organic compounds, electrode materials for rechargeable aqueous zinc-ion batteries, and lithium batteries with different morphologies nanorods/nanowires/nanotubes/nanofibers/nanofelts for non-toxic, low cost and high electrochemical stability, and a high dielectric constant[24-26]. Moreover, the atomic layer deposition (ALD) technique is an outstanding alternative to increasing the dielectric constant from new materials. It was reported that ALD protective films were deposited onto cathode or anode electrode[27,28] and metal oxide films coated onto an electrode for electrical conductivity were tried to introduce in lithium-ion batteries[29,30]. In the supercapacitors, charge-storage films deposited onto electrically conductive electrodes[31].

Herein, a coated high dielectric layer on a complex carbon surface was tried for enhancing dielectric constant in the atomic layer deposition method with vanadium pentoxide. In this method, a well-controlled ultrathin vanadium pentoxide (V_2O_5) film was uniformly formed on the surface of activated carbon based on the sequential use of a gas phase chemical process. The ALD-modified electrode is keeping the properties of surface area and conductivity. Thus, it increased total capacitance by increasing the surface charge density due to the effect of the dielectric constant while minimizing the reduction in surface area.

2. Experimental section

2.1. Atomic Layer Deposition (ALD)

Film deposition was achieved with a lab-made ALD, developed by GASONICS, using nitrogen (99.999%) as a carrier and purging gas. The ALD technique consists of 1) sequentially adding the reaction precursors, which determine the growth state of the deposited film to be controlled by the atomic layer scale with excellent coverage and uniformity of deposition. The vanadium source (vanadyl triisopropoxide $VO(OC_3H_7)_3$ from Sigma Aldrich) was kept at 398 K while the water source (water vapor) was kept at room temperature. To deposit the film, vanadium and water precursors were alternately added into the substrate in the flow of nitrogen carrier gas. The reactor chamber was circulated in nitrogen gas after each precursor added and pulsed. Each deposition was made up to the aimed thickness by alternating the following pulse sequence (cycle): t1/t2/t3/t4, where t1, t2, t3, and t4 were the individual pulse times (in ms) of VTIP, purge (N_2), H_2O and purge (N_2), respectively. The formation of V_2O_5 proceeds from the reaction between the vanadium precursor and water: $2VO(OC_3H_7)_3 + 3H_2O \Rightarrow V_2O_5 + 6HOC_3H_7$. Scanning electron micrographs have shown that the films consist of particles. X-ray diffraction (XRD) patterns of the thin films were carried out using a Co Kα radiation source (Co Kα = 1.7890 Å) at room temperature.

2.2. Materials and electrode preparation

Commercial activated carbon (P-60, Kuraray Co. Ltd.) was used as pristine AC (p-AC) in this experiment. The p-AC was mixed with 10 wt% polyvinylidene fluoride (PVDF, Aldrich Co. Ltd.) and dimethylacetamide (DMAC, Aldrich Co. Ltd.) using stir plate for 2 hours. To prepare the slurry, p-AC and m-AC were homogeneously mixed with 10 wt.% PVDF in a 9:1 weight ratio, respectively. The slurry was then cast onto the graphite sheet (10 cm x 10 cm) using a doctor blade and dried at 60 °C for 10 hours. After we created the electrode using the above method, V_2O_5 was deposited by ALD for preparing modified AC (m-AC). For the ALD of V_2O_5, vanadium (V) triisopropoxide (VTIP, $V(OCH(CH_3)_2)_4$) and water (H_2O) were used as precursors with a nitrogen carrier gas. Through preliminary experiments, we defined the four-point cycles (0, 10, 30 and 50 cycles) as target cycles. In each ALD cycle, two precursors are sequentially released into the reaction chamber. Its cycle consists of continuous exposure to VTIP for 15 s, N_2 for 30 s, water for 10 s and Argon gas purges for 30 s. The same procedure is repeated from 10 to 50 ALD cycles for m-AC.

2.3. Characterization

The surface chemical composition of the m-AC was analyzed using X-ray photoelectron spectroscopy (XPS, VG Multilab 2000). X-ray diffraction (XRD, Rigaku Miniflex II) was also employed to study the bulk crystal structure of the p-AC and m-AC. The morphology and composition change of p-AC and m-AC were observed using field emission scanning electron microscopy (FE-SEM, JEM-2100) and an energy dispersive X-ray spectrometer (EDS, Hitachi S-4700). Specific surface area (SSA) and pore size distribution (PSD) of the p-AC and m-AC were measured using a Brunauer-Emmet-Teller analyzer (BET, Bel Japan Inc. Ltd.). In order to measure the capacitance of p-AC and m-AC, cyclic voltammetry (CV) and electrochemical impedance spectroscopy (EIS) measurements were carried out in 0.5 M NaCl solution using a potentiostat/galvanostat (PGSTAT30, Eco Chemie Inc. Ltd.) with a two-electrode half-cell. The p-AC and m-AC were used as working electrodes, with a carbon electrode as counter electrodes, respectively. The potential was swept between -0.2 V and 0.6 V at dif-

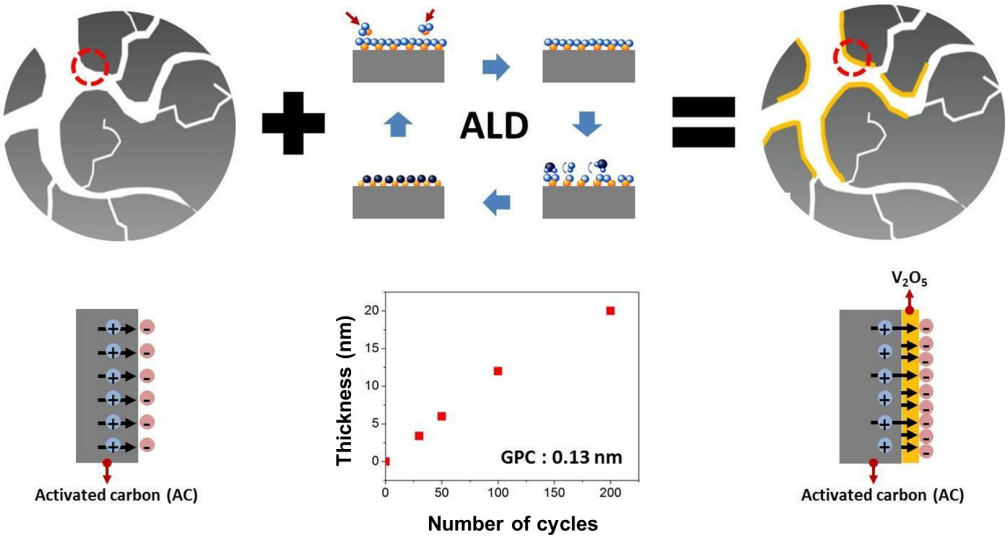

Figure 1. The schematic of V_2O_5 ALD on the AC, dielectric effect and GPC.

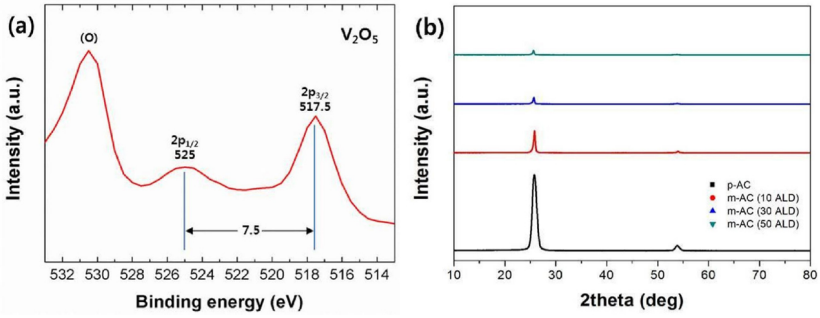

Figure 2. (a) The XPS spectra of V_2O_5, (b) the XRD patterns of m-AC by ALD.

ferent scan rates between 10 and 50 mV s^{-1}. For EIS measurement, the frequency range was from 100 kHz to 10 MHz.

2.4. CDI unit cell tests

The fabricated electrodes were employed as positive and negative electrodes to assemble the CDI unit cell. The electrosorption ability of electrodes was performed in a CDI unit cell, made by current collectors, gaskets, and spacers. The NaCl feed solution (1 mM NaCl) flowed into the CDI cell at various flow rate (10, 20 and 50 mL min^{-1}) during the CDI test. The feed solution has an ionic conductivity of 110 μS cm^{-1}. Ions in the feed solution were adsorbed on the surface of the electrode, applying a fixed potential across the cell (1.5 V). The concentration variation of NaCl solution was measured with a conductivity meter (Model-3200, YSI Inc. Ltd.), and salt removal amount was shown by the average adsorbed NaCl mass in one charging process divided by electrode mass (mg g^{-1}).

3. Results and discussion

3.1. Material characterization

Schematic illustration of our designed CDI electrode using ALD and its function was shown in Figure 1. In contrast to other coating methods, the ALD technique can be deposited very uniformly and thickness controllable. The average growth per cycle (GPC) of V_2O_5 using ALD is 0.13 nm. This GPC is sufficiently small to form a sub-nm-sized layer compared with the macro/mesopore size. Thus, the only surface can be coated with a very thin layer while maintaining the overall surface area. This dielectric constant material increases the electric charge density of the surface resulting from the electrical polarization inside. Therefore, it is expected that V_2O_5 ultrathin layer would improve the electric double-layer capacitance (EDLC) of the carbon electrode in CDI operation.

X-ray analysis techniques are a useful method to analyze the formation of pristine and modified materials. X-ray photoelectron spectroscopy (XPS) measurements were taken after ALD cycles to check the chemical composition of V_2O_5 formed through the ALD. In Figure 2(a), the difference between $V2p_{3/2}$ and the O1s peak, $\Delta BE(V2p_{3/2}-V2p_{1/2})$, a value that agrees with the expected value (7.5 eV) reported in the literature for V_2O_5[5]. Figure 2(b) displays the XRD patterns according to ALD cycles. The diffraction peaks at ~26° correspond to (002) diffraction planes of the hexagonal graphite structure[32]. The m-AC showed a similar peak pattern to p-AC; however, peak intensities in m-AC significantly decreased in accordance with forming V_2O_5 layer which means that the V_2O_5 layer was covered all over the

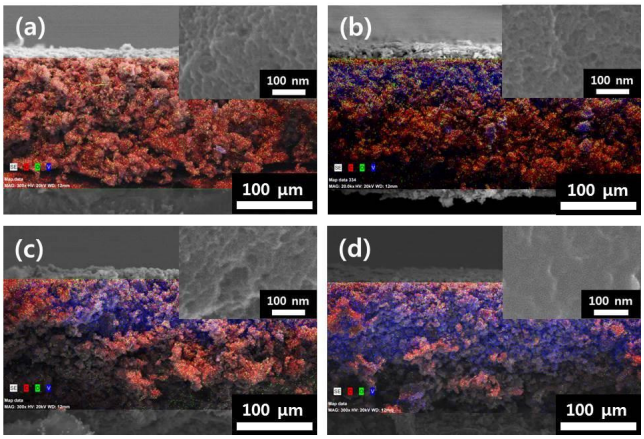

Figure 3. SEM images of side and top view on (a) p-AC, (b) m-AC (10 ALD), (c) m-AC (30 ALD), (d) m-AC (50 ALD) (C- Carbon (red color), O- Oxygen (green color) and V − Vanadium (blue color)).

Table 1. Comparison of Composition Amount by EDS (Unit: atomic %)

	p-AC	m-AC		
		10 cycles	30 cycles	50 cycles
Carbon (C)	94.83	91.56	88.59	85.50
Oxygen (O)	5.16	7.87	10.08	11.12
Vanadium (V)	0.01	0.56	1.34	3.38

surface of a carbon electrode and its crystallinity was amorphous.

Figure 3 shows the surface and cross-sectional morphologies of the p-AC and m-AC in field emission scanning electron microscopy (FE-SEM) and EDS mapping were carried out. It targeted four different layered thickness which were 0, 10, 30, and 50 cycles. Figure 3(a) shows that p-AC has a porous structure with a void about a few tens of nanometer sizes without a vanadium element. However, the distribution and composition of V_2O_5 were increased according to ALD cycles and m-AC after 10, 30, and 50 cycles in Figure 3(b,c and d); it shows a notable difference compared to p-AC. Notably, it was confirmed that vanadium and oxygen portions increase and carbon portions decrease when ALD cycles increase because vanadium and oxygen were covered with carbon substrate in Table 1.

It was shown as the nitrogen adsorption-desorption isotherms and the BET surface area, pore volume and pore size distribution of the obtained p-AC and m-AC in Figure 4 and the data are summarized in Table 2. The mean pore diameter, mostly composed of micropores, are not changed regardless of cycle numbers even though the BET specific surface area deduced from the BJH plot slightly decreased from 1535 $m^2\ g^{-1}$ (p-AC) to 1188 $m^2\ g^{-1}$ (m-AC, 50 ALD) and specific volume also decreased from 0.77 $m^3\ g^{-1}$ (p-AC) to 0.58 (m-AC, 50 ALD), implying that the V_2O_5 layer was mainly formed in the outer surface of meso/macro carbons. An ultrathin layer of V_2O_5 through the ALD enhanced the surface wettability, contributing to the higher capacitance. In Figure 5, the degree of contact angle slightly decreased from 67 to 40°, which implied that the increment of the hydrophilicity causes by the weakness of the surface tension.

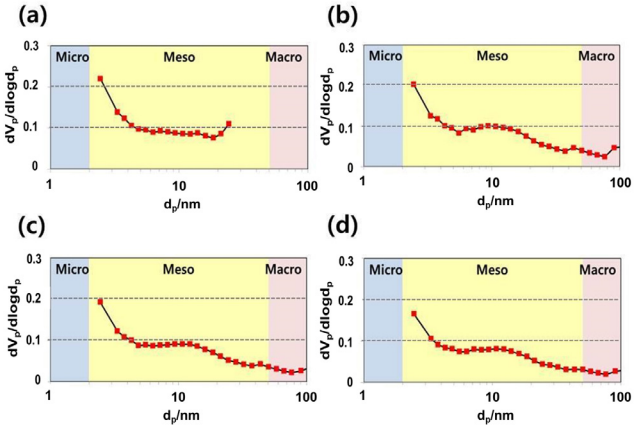

Figure 4. BJH plot of (a) p-AC, (b) m-AC (10 ALD), (c) m-AC (30 ALD), (d) m-AC (50 ALD).

Table 2. Comparison of Specific Surface Area, Specific Volume and Mean Pore Diameter

	p-AC	m-AC		
		10 cycles	30 cycles	50 cycles
Specific surface area (m^2/g)	1535	1478	1380	1188
Specific volume (cm^3/g)	0.77	0.72	0.66	0.58
Mean pore diameter (nm)	2	1.95	1.93	1.95

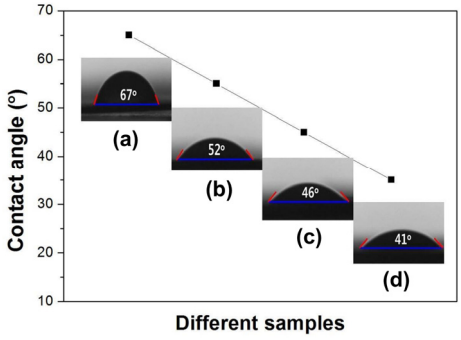

Figure 5. Contact angle of (a) p-AC, (b) m-AC (10 ALD), (c) m-AC (30 ALD), (d) m-AC (50 ALD).

3.2. Electrochemical test

In order to measure the specific capacitance of p-AC, the CVs were measured between - 0.2 V and 0.6 V in 0.5 M NaCl at room temperature using a potentiostat/galvanostat (PGSTAT30, Eco Chemie Inc. Ltd.). The CV was employed to determine the electrochemical properties of the p-AC and m-AC electrodes. The CV curves of the p-AC and m-AC at a scan rate of 10 mV/s are shown in Figure 6(a). The p-AC exhibited a rectangular-shaped CV, corresponding to a specific capacitance of 22.8 F g^{-1} from its double-layer region. On the other hand, m-AC (30 ALD) increased the specific capacitance up to 43.7 F g^{-1}, an almost two-fold rise in capacitance and this reason was the surface charge density due to the coating of dielectric material. The

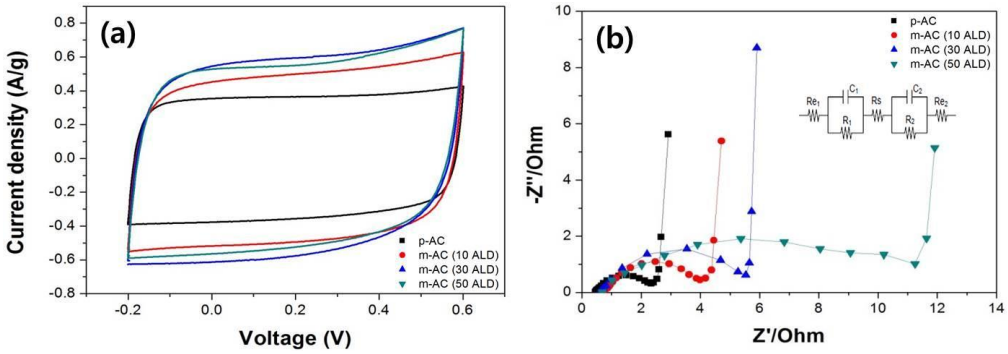

Figure 6. (a) The cyclic voltammograms of a p-AC and m-AC electrode at a scan rate of 10 mV/s and (b) The EIS patterns of p-AC and m-AC.

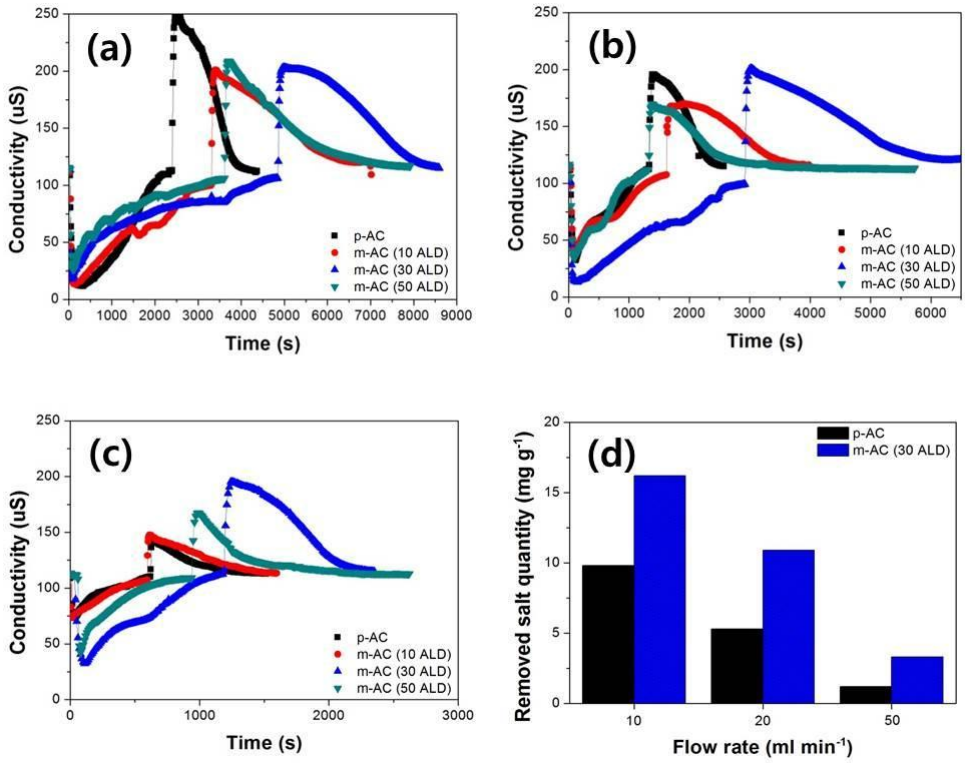

Figure 7. CDI unit cell test at various flow rate (a) 10 mL m^{-1}, (b) 20 mL m^{-1}, (c) 50 mL m^{-1} and (d) comparison of removed salt quantity between p-AC and m-AC (30 ALD).

CV curves of m-AC exhibited a rectangular shape without the redox peaks at a voltage window from -0.2 to 0.6 V, which indicated predominant capacitance with EDLC. The EIS measurement was performed to study the electrochemical frequency behavior and equivalent series resistance (ESR) of the capacitor system. The Nyquist plots of p-AC and m-AC were tested in the frequency range from 10 MHz to 100 kHz. In Figure 6(b), All of the electrodes showed a comparable ESR at around 0.3 Ω, which can be established from the intersection point on the real axis of the Nyquist plots. The semicircle at high frequency explained the interfacial charge transfer resistance and the variation was consistent with specific capacitance. In the low-frequency region, the 45° sloped portion of Warburg impedance revealed the electrolyte ion diffusion behavior[33]. The variation in electrolyte ion diffusion behavior is consistent with that of BET results since low ion diffusion resistances mean short diffusion path lengths of the ions in the electrolyte[34]. In conclusion, the m-AC (30 ALD) showed the best capacitance due to its dielectric constant effect maintaining a large surface area, which rapid ion diffusion and efficient charge transfer.

3.3. CDI unit cell tests

CDI unit cells were assembled and used to evaluate the performance of the carbon electrode for ion removal. Figure 7 shows the ion removal rates of electrodes based on p-AC and m-AC, in terms of the change in the conductivity of feed and effluent solutions. In a typical CDI test, a voltage is applied across the unit cell and ions in the electrolyte are adsorbed on the electrode surface, decreasing the ionic conductivity in the solution. The ionic conductivity of the effluent solution eventually increases with time due to saturation. The electrosorption

capacity was defined as the adsorbed ion amounts per gram of electrode. Also, it can be calculated by the conductivity variation of solutions during the charging process. The m-AC as the electrode was tested in the CDI unit cell. Conductivity transients in solutions during the charging process at different flow rates with an initial conductivity of 110 μS/cm. Once the potential was applied, the cation and anion are adsorbed onto the surface of the oppositely charged electrodes. The electrical conductivity of the NaCl solution dramatically decreased at the starting point in the CDI processes. It was evident that the CDI process is closely associated with the flow rate. With the increase in flow rate from 10 to 50 mL min^{-1}, the ionic adsorption efficiency became lower due to the decrease in residence time and the total electrosorption capacity gradually decreased from 9.8 mg g^{-1} to 1.2 mg g^{-1}. Compared to the p-AC, the m-AC electrode possessed a relatively higher electrosorption capacity. Notably, in the case of m-AC (30 ALD), it showed 165% and 205%, 275%, respectively at various flow rates (10, 20 and 50 mL min^{-1}). These results are very significant because a high proportion of the EDLC formed in the pores near the surface as the speed of the flow increases. It can be explained by the more surface electric charge density in macro/mesopores, which can have strong electrostatic interactions with the electrodes in the presence of the applied electric field. The results showed that the m-AC (30 ALD) electrode has more of an advantage in the CDI process.

4. Conclusion

The ultrathin layer of V_2O_5 on activated carbon was successfully prepared with different numbers of ALD cycles (0, 10, 30, and 50). The material prepared with 30 cycles of V_2O_5 ALD showed significant enhancement in EDLC compared to pristine-activated carbon (p-AC). The physical changes of surface composition enhanced the electric double-layer capacitance of AC, following the increasing of electric charge density as well as increasing wettability for adsorption on the electrode surface. These properties led to improved CDI performance of m-AC in terms of ion removal efficiency and capacity compared with p-AC. The findings of this work can provide evidence on the potential of m-AC in water desalination and softening applications.

Declarations

The authors declare that they have no known competing financial interests or personal relationships that could have influenced the work reported in this paper.

Acknowledgment

This work was also supported by the GIST Research Institute (GRI) grant funded by the GIST in 2022.

References

1. J. Oladunni, J. H. Zain, A. Hai, F. Banat, G. Bharath, and E. Alhseinat, A comprehensive review on recently developed carbon based nanocomposites for capacitive deionization: From theory to practice, *Sep. Purif. Technol*,. **207**, 291-320 (2018).
2. Y. Oren, Capacitive deionization (CDI) for desalination and water treatment — past, present and future (a review), *Desalination*, **228**, 10-29 (2008).
3. M. A. Anderson, A. L. Cudero, and J. Palma, Capacitive deionization as an electrochemical means of saving energy and delivering clean water, Comparison to present desalination practices: Will it compete? *Electrochim. Acta*, **55**, 3845-3856 (2010).
4. S. Porada, R. Zhao, A. van der Wal, V. Presser, and P. M. Biesheuvel, Review on the science and technology of water desalination by capacitive deionization, *Prog. Mater. Sci.*, **58**, 1388-1442 (2013).
5. H. Helmholtz, Ueber einige Gesetze der Vertheilung elektrischer Ströme in körperlichen Leitern mit Anwendung auf die thierisch-elektrischen Versuche, *Ann. Phys.*, **165**, 211-233 (1853).
6. B. A. Fellman, M. Atieh, and E. N. Wang, Carbon-based electric double layer capacitors for water desalination, *ASME 2010 8th International Conference on Nanochannels, Microchannels, and Minichannels Collocated with 3rd Joint US-European Fluids Engineering Summer Meeting* **Issue PARTS A AND B**, 275-279 (2010).
7. J. Farmer, D. Fix, and G. Mack, Capacitive deionization of water: An innovative new process, *Proceedings of the International Conference on Radioactive Waste Management and Environmental Remediation* **2**, 1215-1220 (1995).
8. L. Khezami, A. Chetouani, B. Taouk, and R. Capart, Production and characterisation of activated carbon from wood components in powder: Cellulose, lignin, xylan, *Powder Technol.*, **157**, 48-56 (2005).
9. M. K. B. Gratuito, T. Panyathanmaporn, R.-A. Chumnanklang, N. Sirinuntawittaya, and A. Dutta, Production of activated carbon from coconut shell: Optimization using response surface methodology, *Bioresour. Technol.*, **99**, 4887-4895 (2008).
10. A. L. Ahmad, M. M. Loh, and J. A. Aziz, Preparation and characterization of activated carbon from oil palm wood and its evaluation on Methylene blue adsorption, *Dyes Pigm.*, **75**, 263-272 (2007).
11. H. Teng, T.-S. Yeh, and L.-Y. Hsu, Preparation of activated carbon from bituminous coal with phosphoric acid activation, *Carbon*, **36**, 1387-1395 (1998).
12. R. Kumar, S. Sen Gupta, S. Katiyar, V. K. Raman, S. K. Varigala, T. Pradeep, and A. Sharma, Carbon aerogels through organo-inorganic co-assembly and their application in water desalination by capacitive deionization, *Carbon*, **99**, 375-383 (2016).
13. P. Xu, J. E. Drewes, D. Heil, and G. Wang, Treatment of brackish produced water using carbon aerogel-based capacitive deionization technology, *Water Res.*, **42**, 2605-2617 (2008).
14. H. Li, L. Zou, L. Pan, and Z. Sun, Novel Graphene-Like Electrodes for Capacitive Deionization, *Environ. Sci. Technol.*, **44**, 8692-8697 (2010).
15. H. Li, T. Lu, L. Pan, Y. Zhang, and Z. Sun, Electrosorption behavior of graphene in NaCl solutions, *J. Mater. Chem.*, **19**, 6773-6779 (2009).
16. H. Li, L. Zou, L. Pan, and Z. Sun, Using graphene nano-flakes as electrodes to remove ferric ions by capacitive deionization, *Sep. Purif. Technol.*, **75**, 8-14 (2010).
17. L. Wang, M. Wang, Z.-H. Huang, T. Cui, X. Gui, F. Kang, K.

Wang, and D. Wu, Capacitive deionization of NaCl solutions using carbon nanotube sponge electrodes, *J. Mater. Chem.*, **21**, 18295-18299 (2011).
18. C. Nie, L. Pan, Y. Liu, H. Li, T. Chen, T. Lu, and Z. Sun, Electrophoretic deposition of carbon nanotubes-polyacrylic acid composite film electrode for capacitive deionization, *Electrochim. Acta*, **66**, 106-109 (2012).
19. Y. Wang, L. Zhang, Y. Wu, S. Xu, and J. Wang, Polypyrrole/carbon nanotube composites as cathode material for performance enhancing of capacitive deionization technology, *Desalination*, **354**, 62-67 (2014).
20. Y. Wang, R. Wang, S. Xu, Q. Liu, and J. Wang, Polypyrrole/polyaniline composites with enhanced performance for capacitive deionization, *Desalin. Water Treat.*, **54**, 3248-3256 (2015).
21. W.-Y. Huang, J. Wang, Y.-M. Liu, Q.-S. Zheng, and C.-Y. Li, Inhibitory effect of Malvidin on TNF-α-induced inflammatory response in endothelial cells, *Eur. J. Pharmacol.*, **723**, 67-72 (2014).
22. X. Song, H. Liu, L. Cheng, and Y. Qu, Surface modification of coconut-based activated carbon by liquid-phase oxidation and its effects on lead ion adsorption, *Desalination*, **255**, 78-83 (2010).
23. C. Y. Yin, M. K. Aroua, and W. M. A. W. Daud, Review of modifications of activated carbon for enhancing contaminant uptakes from aqueous solutions, *Sep. Purif. Technol*. **52**, 403-415 (2007).
24. Y. Li, Z. Huang, P. K. Kalambate, Y. Zhong, Z. Huang, M. Xie, Y. Shen, and Y. Huang, V_2O_5 nanopaper as a cathode material with high capacity and long cycle life for rechargeable aqueous zinc-ion battery, *Nano Energy*, **60**, 752-759 (2019).
25. B. Jeon, C. Ko, A. C. T. van Duin, and S. Ramanathan, Chemical stability and surface stoichiometry of vanadium oxide phases studied by reactive molecular dynamics simulations, *Surf. Sci.*, **606**, 516-522 (2012).
26. X. Liu, J. Zeng, H. Yang, K. Zhou, and D. Pan, V_2O_5-Based nanomaterials: synthesis and their applications, *RSC Adv.*, **8**, 4014-4031 (2018).
27. Y. S. Jung, A. S. Cavanagh, L. A. Riley, S.-H. Kang, A. C. Dillon, M. D. Groner, S. M. George, and S.-H. Lee, Ultrathin direct atomic layer deposition on composite electrodes for highly durable and safe Li-ion batteries, *Adv. Mater.*, **22**, 2172-2176 (2010).
28. Y. S. Jung, A. S. Cavanagh, A. C. Dillon, M. D. Groner, S. M. George, and S.-H. Lee, Enhanced stability of $LiCoO_2$ cathodes in lithium-ion batteries using surface modification by atomic layer deposition, *J. Electrochem. Soc.*, **157**, A75 (2009).
29. D. M. Piper, J. J. Travis, M. Young, S.-B. Son, S. C. Kim, K. H. Oh, S. M. George, C. Ban, and S.-H. Lee, Reversible high-capacity si nanocomposite anodes for lithium-ion batteries enabled by molecular layer deposition, *Adv. Mater.*, **26**, 1596- 1601 (2014).
30. Y. He, D. M. Piper, M. Gu, J. J. Travis, S. M. George, S.-H. Lee, A. Genc, L. Pullan, J. Liu, S. X. Mao, J.-G. Zhang, C. Ban, and C. Wang, In situ transmission electron microscopy probing of native oxide and artificial layers on silicon nanoparticles for lithium ion batteries, *ACS Nano*, **8**, 11816-11823 (2014).
31. M. J. Young, A. M. Holder, S. M. George, and C. B. Musgrave, Charge storage in cation incorporated α-MnO_2, *Chem. Mater.*, **27**, 1172-1180 (2015).
32. Z. Peng, D. Zhang, L. Shi, T. Yan, S. Yuan, H. Li, R. Gao, and J. Fang, Comparative electroadsorption study of mesoporous carbon electrodes with various pore structures, *J. Phys. Chem. C*, **115**, 17068-17076 (2011).
33. K.-K. Park, J.-B. Lee, P.-Y. Park, S.-W. Yoon, J.-S. Moon, H.-M. Eum, and C.-W. Lee, Development of a carbon sheet electrode for electrosorption desalination, *Desalination*, **206**, 86-91 (2007).
34. S. Chung, J. K. Lee, J. D. Ocon, Y.-I. Son, and J. Lee, Carbon electrodes in capacitive deionization process, *Appl. Chem. Eng.*, **25**, 346-351 (2014).

Authors

Sangho Chung; Ph.D., Senior Researcher, School of Earth Sciences and Environmental Engineering, Gwangju Institute of Science and Technology, Gwangju 61005, Korea; swfs1@gist.ac.kr

Sungyool Bong; Ph.D., Research Associate Professor, School of Earth Sciences and Environmental Engineering, Gwangju Institute of Science and Technology, Gwangju 61005, Korea; saraph04@gist.ac.kr

Jaeyoung Lee; Dr. rer. nat., Full Professor, School of Earth Sciences and Environmental Engineering, Gwangju Institute of Science and Technology, Gwangju 61005, Korea; jaeyoung@gist.ac.kr